6.06 Lithosphere Stress and Deformation

M. L. Zoback, US Geological Survey, Menlo Park, CA, USA

M. Zoback, Stanford University, Stanford, CA, USA

Published by Elsevier B.V.

6.06.1 Introduction

The advent of plate tectonics brought a new meaning and understanding to the mechanically defined lithosphere. Lithosphere became synonymous with the Earth's outer thermal boundary, the mobile 'plates' of plate tectonics. Motion of the plates was soon understood to be the result of a balance of forces that both drove and resisted their movement. While convection in the Earth is the ultimate source of the energy to drive plate tectonics, large density inhomogeneities associated with plate subduction and generation of new oceanic lithosphere create the major driving forces. Other potentially important forces include viscous drag at the base of plates (either driving or resisting) as well as frictional resistance along plate boundaries.

Lithospheric deformation, the 'tectonics' of plate tectonics, is a result of the stress state within the lithosphere. In this chapter we review the evidence for, and the implications of, field and laboratory data on the state of stress in the lithosphere and the forces acting upon and within it. Intensive investigation over the past few decades has revealed that the lithospheric state of stress is remarkably uniform both with depth and over vast regions of plate interiors. The broad uniformity of observed stress orientations and relative magnitudes, even across major bends in old orogenic belts, indicates that the lithospheric stress field is the result of present-day forces and is not due to residual stresses from past tectonic activity. Modeling has shown us that the same forces acting on and within the plates to drive plate motion are the same forces responsible for the state of stress in the lithosphere. Direct measurement of stress magnitudes at depth confirms a simple model in which stress differences in the crust are close to and limited by the frictional strength of the most well-oriented faults.

In contrast to the relative uniformity of intraplate stress fields, deformation rates in plate interiors vary by about eight orders of magnitude. We show how knowledge of the stress field, combined with mechanical, thermal, and rheological properties, can be used to constrain both the rate and style of lithospheric deformational processes.

6.06.2 Global Patterns of Tectonic Stress

Early attempts to map the state of stress in lithosphere were largely based on earthquake focal mechanisms and very sparse, and usually quite shallow, *in situ* stress measurements (e.g., Raleigh, 1974; Richardson *et al.*, 1976, 1979; Pavoni, 1961, 1980). Despite a relatively low density of stress data, these early investigations hinted at broad-scale uniformity of stresses. In 1980, Zoback and Zoback introduced an integrated stress mapping strategy utilizing a variety of geologic and geophysical data: earthquake focal plane mechanisms, young geologic data on fault slip and volcanic alignments, *in situ* stress measurements, and stress-induced wellbore breakouts, and drilling-induced tensile fractures. The initial effort to apply this integrated mapping strategy to the conterminous United States (Zoback and

Zoback, 1980) revealed two fundamental characteristics of the crustal stress field:

1. To first order, the stress field is uniform with depth throughout the upper brittle crust as indicated by the consistency of stress orientations inferred from the different data types that sampled different volumes of rock at different depths: geologic and *in situ* stress measurement data sampled the surface or very near surface (less than 1–2 km depth), earthquake focal mechanisms provide coverage for depths between about 5 and 20 km, whereas wellbore breakout and drilling-induced fracture data commonly sample 1–4 km deep and in some cases as deep as 5–6 km, providing a valuable link between the near-surface and the focal mechanism data.
2. Stress orientations are remarkably uniform over broad regions (length scales up to thousands of kilometers), despite large changes in crustal geology, tectonic history, and crustal thickness.

A brief description of how the state of stress is inferred from the different types of stress indicators used is given in Appendix 1: More information on the assumptions, difficulties, and uncertainties of inferring stress orientations from these different data types can be found in Zoback and Zoback (1980, 1991), Zoback *et al.* (1989).

A quality-ranking scheme was developed by Zoback and Zoback (1989, 1991) to assess how reliably an individual determination records the tectonic stress field. The quality-ranking scheme also permits comparison of orientations inferred from very different types of stress indicators that sample different depth intervals. This quality criterion was subsequently utilized in the International Lithosphere Program's World Stress Map Project, a large collaborative effort of data compilation and analyses by over 40 scientists from 30 different countries (Zoback, 1992). A special issue of the *Journal of Geophysical Research* (vol. 97, pp. 11703–12014) summarized the overall results of this project as well as presented the individual contributions of many of these investigators in various regions of the world. Today, the World Stress Map (WSM) database includes more than 10 000 entries and is maintained by a Research Group of the Heidelberg Academy of Sciences and Humanities.

The global stress orientation data continue to reveal striking regional uniformity (**Figure 1(a)**). The success of the WSM project has validated this integrated stress mapping strategy using a variety of data types and demonstrated that with careful attention to data quality, coherent stress patterns over large regions of the Earth can be mapped with reliability and interpreted with respect to large-scale lithospheric processes.

Similar to stress orientations, stress regime (relative magnitude of the three principal stresses) also shows marked regional uniformity. Because stress is a tensor quantity, a full description of the state of stress requires information on both magnitudes and orientation. Direct stress measurements at depth as well as the style of faulting at depth revealed by earthquakes indicates that, in general, the state of stress at depth can be described by three principal stresses ($S_1 > S_2 > S_3$) that lie in approximately horizontal and vertical planes (e.g., Zoback and Zoback, 1989; Zoback, 1992). The magnitude of the vertical principal stress is generally taken as the weight of the overburden.

Following Anderson (1951) in his classic paper on faulting, we define stress regime by the relative magnitude of the vertical stress (S_v) to the two maximum and minimum horizontal stresses (respectively, S_{Hmax} and S_{hmin}). Three distinct regimes are possible:

- *Normal faulting stress regime* When the vertical stress dominates ($S_1 = S_v$), gravity drives normal faulting and creates horizontal extensional deformation:

$$S_v > S_{Hmax} > S_{hmin} \quad [1]$$

- *Reverse faulting stress regime* When both horizontal stresses exceed the vertical stress ($S_3 = S_v$) compressional deformation and shortening is accommodated through thrust or reverse faulting:

$$S_{Hmax} > S_{hmin} > S_v \quad [2]$$

- *Strike-slip faulting stress regime* An intermediate stress state ($S_2 = S_v$), where the difference between the two horizontal stresses (horizontal shear) dominates deformation, resulting in strike-slip faulting:

$$S_{Hmax} \geq S_v \geq S_{hmin} \quad [3]$$

Relative stress magnitude information can be obtained from direct *in situ* stress measurements as well as from the style of tectonic faulting inferred from earthquake focal mechanisms and

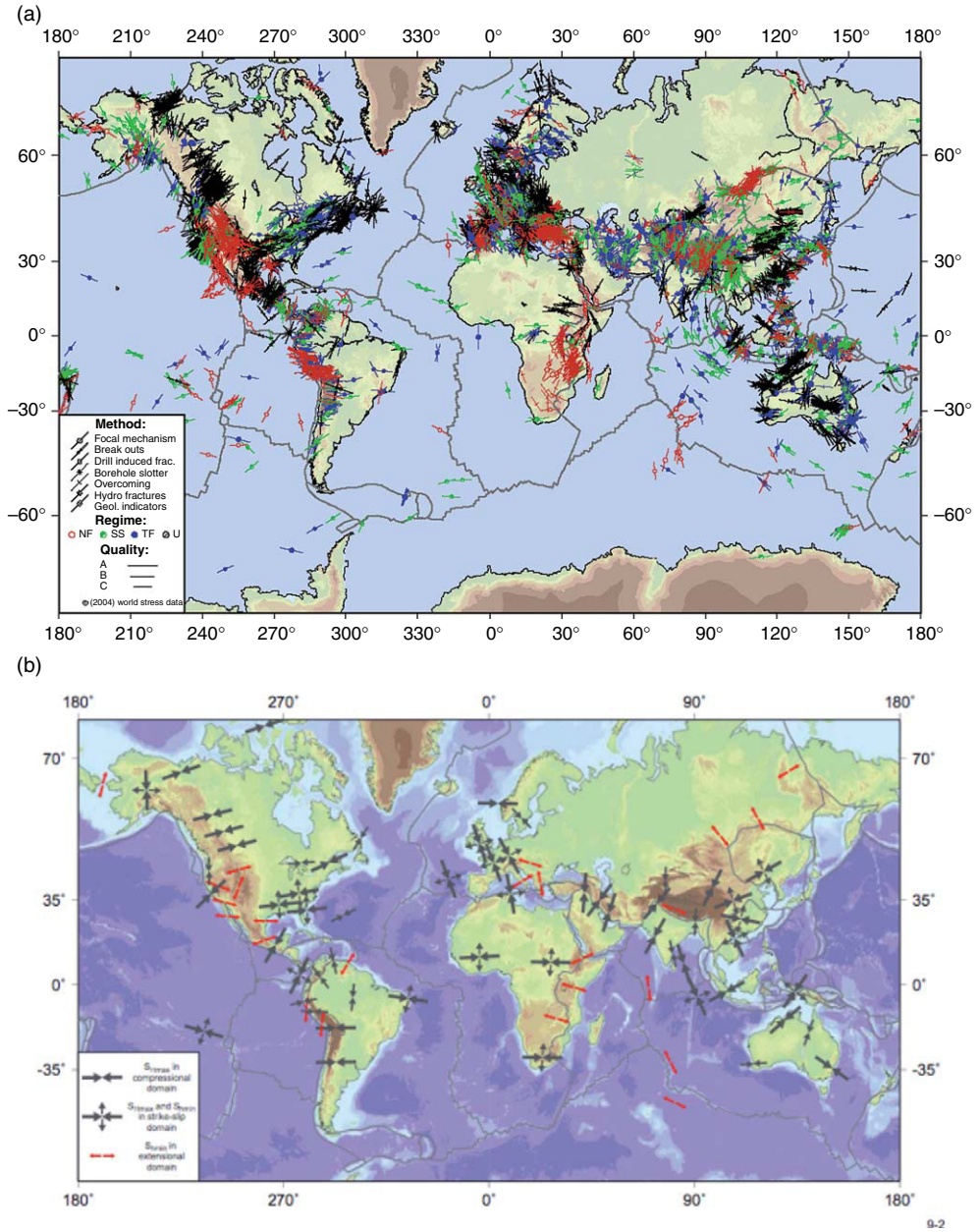

Figure 1 (a) Maximum horizontal stress orientations from the World Stress Map project plotted on a base of average topography. Line lengths of data are proportional to quality. Stress regime are indicated by color: red, normal faulting; green strike-slip faulting; blue, reverse faulting. (b) Generalized stress map mean stress directions based on averages of clusters of data shown in **Figure 1(a)**. A single set of thick inward-pointing arrows indicate S_{Hmax} orientations in a reverse faulting stress regime. A single set of outward-pointing arrows indicate S_{hmin} orientations in a normal faulting stress regime. Strike-slip faulting stress regime indicated by thick-inward-pointing arrows (S_{Hmax} direction) and thin outward-pointing arrows (S_{hmin} direction). Symbol sizes in all cases are proportional to the number and consistency of data orientations averaged from World Stress Map project. Reproduced from Zoback ML (1992) First- and second-order patterns of strees in the lithosphere: The World Stress Map project. *Journal of Geophysical Research* 97: 11703–11728, with permission from American Geophysical Union. (The current version of the World Stress Map database can be found at: http://www-wsm.physik.uni-karlsruhe.de/.)

geologic observations of young faulting. While global coverage is quite variable, the relative uniformity of both stress orientation and relative magnitudes in different parts of the world is striking and permits mapping of regionally coherent tectonic stress regimes.

Figure 1(b) presents a generalized version of the Global Stress Map that is quite similar to that presented by Zoback (1992). Tectonic stress regimes are indicated in **Figure 1(b)** by both color and arrow type. Blue inward-pointing arrows indicate S_{Hmax} orientations in areas of compressional (strike-slip and thrust) stress regimes. Red outward-pointing arrows give S_{hmin} orientations (extensions direction) in areas of normal faulting regimes. Regions dominated by strike-slip tectonics are distinguished with green thick inward-pointing, and orthogonal, thin outward-pointing, arrows. Overall, arrow sizes on **Figure 1(b)** represent a subjective assessment of 'quality' related to the degree of uniformity of stress orientation and also to the number and density of data (Zoback, 1992).

The data shown in **Figures 1(a)** and **1(b)** reinforce the broad-scale patterns and general conclusions regarding the global database summarized in Zoback *et al.* (1989):

- The interior portions of most plates (variously called intraplate and mid-plate regions) are dominated by compression (thrust and strike-slip stress regimes) in which the maximum principal stress is horizontal.
- Active extensional tectonism (normal faulting stress regimes) in which the maximum principal stress is vertical generally occurs in topographically high areas in both the continents and the oceans.
- Regional consistency of both stress orientations and relative magnitudes permits the definition of broad-scale regional stress provinces, many of which coincide with physiographic provinces, particularly in tectonically active regions. These provinces may have lateral dimensions on the order of 10^3–10^4 km, many times the typical lithosphere thickness of 100–300 km.

Zoback (1992) referred to these broad regions subjected to uniform stress orientation or a uniform pattern of stress orientation (such as the radial pattern of stress orientations in China) as 'first-order' stress provinces. For example, the uniform ENE S_{Hmax} orientation in mid-plate North America covers nearly the entire continental portion of the plate lying at an average elevation of less than 1000 m (excluding the west coast), and may also extend across much of the western Atlantic basin (Zoback *et al.*, 1986). Thus, here the stress field is uniform over roughly 5000 km in both an E–W direction and an N–S direction. As we will see in Section 6.06.3, most of these first-order stress fields are consistent with the balance of forces acting and within the plates which drive plate motions.

Once the first-order stress patterns are recognized, so called 'second-order' patterns or local perturbations can be identified (Zoback, 1992). These second-order stress fields are often associated with specific geologic or tectonic features; for example, lithospheric flexure, lateral strength contrasts, as well as the lateral density contrasts within the lithosphere which give rise to buoyancy forces derived from lateral variations in gravitational potential energy (e.g., Artyushkov, 1974; Fleitout and Froidevaux, 1982, 1983; Sonder, 1990; Fleitout, 1991; Wortel *et al.*, 1991; Coblentz *et al.*, 1994; Jones *et al.*, 1996; Bai *et al.*, 1992; Zoback and Mooney, 1993). These second-order stress patterns typically have wavelengths ranging from 5 to 10 (or more) times the thickness of the brittle upper lithosphere.

Stress mapping has shown a number of second-order processes that can produce rotations of S_{Hmax} orientations. Few examples include

- A 75–85° rotation on the northeastern Canadian continental shelf possibly related to margin-normal extension derived from sediment-loading flexural stresses (Zoback, 1992).
- An ~45° rotation of stress directions along the mid-Norwegian margin, apparently due to lithospheric flexure associated with deglaciation (see Grollimund and Zoback, 2000).
- A 50–60° rotation within the East African Rift relative to western Africa due to extensional buoyancy forces caused by lithospheric thinning (Zoback, 1992), and an approximately 90° rotation along the northern margin of the Paleozoic Amazonas Rift in central Brazil (Zoback and Richardson, 1996). In this final example, this rotation is hypothesized as being due to deviatoric compression oriented normal to the rift axis resulting from local lithospheric support of a dense mass in the lower crust beneath the rift ('rift pillow').
- An ~50° counter-clockwise rotation of S_{Hmax} directions in the southern San Joaquin basin of California that is associated with the 'big bend' of the San Andreas Fault (Castillo and Zoback, 1995).
- A clockwise rotation of horizontal principal stress directions (and a progressive decrease in horizontal stress magnitudes) going clockwise around the northern boundary of South America. This large-scale rotation of stress directions appears to be at least in part associated with the gravitational effect of a section of the Caribbean Plate subducted to the south beneath continental S. America (Colmenares and Zoback, 2003).

An even larger-scale example of a 'second-order' stress rotation can be found in the stress orientations in much of the westernmost United States which are consistent with the combined effects of right-lateral shear along the San Andreas Plate Boundary and extensional buoyancy forces driven by the topographically high regions of the western United States (e.g., Zoback and Thompson, 1978). Flesch *et al.* (2000) have shown with lithospheric deformational modeling that this superposition is capable' of explaining the north–northeast maximum horizontal orientations and relative magnitudes, and can also predict the rates of deformation. This final example demonstrates that much can be learned by using the observed stress data to constrain the sources of stress acting on the lithosphere (as discussed in a later section). It also demonstrates that large-scale lithospheric heterogeneities can be as important as plate-driving forces in determining the state of stress within the plates (e.g., Humphreys and Coblentz, 2007).

6.06.3 Sources of the Lithospheric Stress Field

The most likely sources of the observed, regionally uniform first-order patterns of stress orientations and relative magnitudes are the large-scale forces acting on and within the plates to drive their motion. Solomon *et al.* (1975) and subsequent studies by Richardson *et al.* (1976, 1979) were the first to attempt to predict global intraplate stress orientations and relative magnitudes by modeling plate-driving forces. Following Forsyth and Uyeda (1975) and Chapple and Tullis (1977) the forces they considered included

- constant value forces acting generally perpendicular to plate boundaries – ridge push (a symmetric force at ridges creating compression far within the plates), slab pull (the balance of the negative buoyancy of the subducting slab and the viscous and frictional resistance to subduction), trench suction (a tractions on plates induced by mantle flow moving toward downwelling at subduction zones), and collisional resistance and
- tractions on the base of plates – drag forces proportional to plate velocity.

For a detailed discussion of each of the above plate-driving forces, see Chapter 6.02.

These forces were incorporated in thin-shell finite-element models of constant-thickness lithosphere to calculate internal stresses in the plates. Richardson *et al.* (1979) constrained their results by a relatively sparse sampling of the global stress field based on earthquake focal mechanisms. They concluded that ridge push and net slab pull were of comparable size and that shear tractions on the base of the plates were resistive.

Zoback *et al.* (1989) showed a correlation between S_{Hmax} orientation and the azimuth of both absolute and relative plate velocities for several intraplate regions. However, Richardson (1992) demonstrated that the ridge push torque pole is very similar to the absolute velocity pole for most plates; thus, a comparison with absolute velocity trajectories can do little to distinguish between ridge push and basal drag as a source of stress. In fact, comparison between stress directions and local azimuths computed from velocity poles is an overly simplistic approach to evaluating the influence of plate-driving force on the intraplate stress field. At best, these correlations demonstrate the important role of the plate boundary forces and can be used to conclude that the net balance of forces driving the plates also stresses them (Zoback *et al.*, 1989).

As the intraplate stress database improved, a number of single-plate finite-element models were produced, following a similar approach to Richardson *et al.* (1979) and assuming a no-net torque constraint. (Richardson, 1978; Richardson and Cox, 1984; Cloetingh and Wortel, 1985, 1986; Richardson and Reding, 1991; Stefanick and Jurdy, 1992; Meijer and Wortel, 1992; Whittaker *et al.*, 1992; Grunthal and Stromeyer, 1992; Coblentz and Sandiford, 1994; Coblentz and Richardson, 1996; Meijer *et al.*, 1997; Coblentz *et al.*, 1998; Flesch *et al.*, 2000; Govers and Meijer, 2001). In many of these models the ridge push force was often used to calibrate the magnitude of all forces acting on the plates as ridge push is the best quantified of the driving forces since it can be calculated directly from bathymetry and the crust/lithosphere structure in the oceans. Over time, these models became increasingly more sophisticated and incorporated gravitational potential energy forces (so-called 'buoyancy forces') within the plates related to lateral variations in lithospheric density and/or thickness (including realistic representations of ridge push force).

Most studies found ridge push to be a significant force and concluded that internal buoyancy body forces due to lateral variations in lithospheric

structure and density (lithospheric buoyancy) were also significant. Some studies found significant compressive stress transmitted across convergent margins and transforms, others found drag to be an important balancing force, either resistive or driving, often depending on how the drag force was formulated (e.g., restricted only to continental portions of plates). The influence of slab pull on the intraplate stress field was generally found to be no larger than (and sometimes smaller than) the magnitude of the other forces acting on the plates. While such models are illuminating, they generally suffer from the lack of well-constrained boundary conditions. Hence, the results of single-plate stress modeling tend to be rather nonunique.

Lithospheric buoyancy forces arise from lateral variations in both crust and mantle-lid thickness. As pointed out by Fleitout and Froidevaux (1982, 1983) regions of high topography (due either to thick crust or thin mantle lid) have high potential energy, hence have a tendency to 'spread' or extend. In contrast, thick, cold mantle lid tends to 'sink' into less-dense asthenosphere, generating compression within the upper lithosphere. Several lines of evidence indicate that buoyancy forces due to inhomogeneities in lithospheric density structure can be significant and comparable in magnitude to plate-driving forces.

1. Ridge push (recognized as a key force in determining stress orientation in a number of plates, particularly those with no attached slab) is actually a buoyancy force acting over the entire profile of cooling oceanic lithosphere.
2. The dominance of extensional tectonics in tectonically active areas at high elevations ($>\sim$2 km) (e.g., the western United States, the East African Rift System, and the Baikal Rift) indicates that positive buoyancy forces (positive potential energy) derived from unusually low densities in the upper mantle (and/or thin lithosphere) are probably the primary force in these regions, overcoming general intraplate compression (Zoback and Mooney, 2003).
3. As noted earlier, Flesch *et al.* (2000) demonstrated that stress orientations in the western US are consistent with a balance of right-lateral shear along the San Andreas Plate Boundary and extensional buoyancy forces generated by the elevated crust and thin lithosphere beneath the western Cordillera.

Over the past two decades significant advances in our understanding of the crustal stress field have been matched by greatly increased knowledge of the three-dimensional (3-D) structure and lateral variations and inhomogeneities in the lithosphere as well as structure and physical properties inferred from tomographic and other seismic studies. This increased knowledge of Earth structure has been incorporated in modeling stress patterns within the plates using basal shear tractions determined from mantle flow models. Bai *et al.* (1992) were the first to attempt a combined approach that predicted both plate velocities and the stresses within plates using a relatively low-resolution model of mantle density anomalies to induce flow in a Newtonian viscous mantle. Bai *et al.* also included buoyancy forces within the lithosphere induced by variations of Moho depth. They imposed a no-net torque constraint to compute plate velocities; these velocities were then used as the shear tractions on the base of the plates to determine internal stresses. Their models showed a relatively poor correlation between the predicted stress directions and the observed regional stress field, possibly due to the coarse spacing (15°) of their grid. However, their models were the first to really investigate the importance of sublithospheric density anomalies on the upper lithosphere stress field.

Bird (1998) implemented a global model in which laterally heterogeneous plates of nonlinear rheology were separated by faults with low friction. He found that driving forces that result only from elevation differences between ocean ridges and trenches (balanced by passive basal drag and fault friction) are not compatible with observed plate velocities. His best models to match both stress orientations and plate velocities required forward drag acting on the continents only, with dense descending slabs pulling oceanic plates and stirring the more viscous mantle. Steinberger *et al.* (2001) also attempted to match plate velocities and stress orientations by calculating a mantle flow field from density structures inferred from seismic tomography. In this model, computed stresses also included the effects of buoyancy forces within the lithosphere due to lateral variations in lithospheric and crustal density and structure. However, their results were somewhat equivocal. While mantle flow models were found to be generally in accord with observed stress directions and plate motion, they also predicted stress directions in the absence of any effects of mantle flow which explained the stress observations nearly as well.

In a comprehensive study, Lithgow-Bertelloni and Guyunn (2004) attempted to match the observed intraplate stress patterns with a set of 3-D global finite-element models that included mantle flow,

lithospheric heterogeneity, and topography. They tested two versions of lithospheric heterogeneity – one based directly on seismic and other constraints (Crust 2.0, Laske *et al.* (2002)) and another assuming a simple model of isostatic compensation. They also implemented mantle tractions computed from two models of mantle density heterogeneity – one based on the history of subduction for the last 180 Myr (which successfully reproduces the present-day geoid and Cenozoic plate velocities) and a second inferred from seismic tomography (Grand *et al.*, 1997). Furthermore, they investigated effects of variable viscosity structure, including the case of a low-viscosity channel between 100 and 200 km depth. The results of this study are also somewhat equivocal. Their mantle traction-only models consistently predict large extensional stresses in the center of the Pacific Plate and over much of the Atlantic – in sharp contrast to the compressional tectonism in these areas inferred from intraplate earthquake focal mechanisms (e.g., Wiens and Stein, 1985). Because their predicted stresses from mantle tractions are a factor two to four times greater than stresses due to lithospheric structure (i.e., buoyancy forces), even when they combine the two sources, the predicted stress field does not match large-scale features of the observed stresses very well, particularly in the oceans. They found the best fits for the observed stress field were predicted from models of lithosphere heterogeneity alone (these models include ridge push forces as it is a buoyancy force resulting from lateral variations of density and structure within the lithosphere).

Zoback and Mooney (2003) implemented a simple model tying lithosphere buoyancy to surface elevation to predict stress regime within continental plate interiors. They determined the crustal portion of lithospheric buoyancy (density × thickness) using the USGS global database of crustal structure determinations (Mooney *et al.*, 2002; Chapter 1.11). Adopting a mid-ocean ridge as a reference column (following Lachenbruch *et al.* (1985) and Lachenbruch and Morgan (1990)) they computed elevations due only to the crustal component of buoyancy and found the predicted elevations exceed observed elevations in nearly all cases (97% of the data), consistent with the existence of a cool lithospheric mantle lid denser than the asthenosphere on which it floats. The difference between the observed and predicted crustal elevation is a measure of the decrease in elevation produced by the negative buoyancy of the mantle lid. This negative buoyancy was combined with a simple thermal model for the density of the mantle lid to compute mantle-lid thickness. They then computed gravitational potential energy differences relative to mid-ocean ridges by taking a vertical integral over the computed complete lithosphere density structure. Their results are shown in **Figure 2(a)** and show broad agreement with observed stress regime data, given in **Figure 2(b)**. They found that thick mantle roots beneath shields lead to strong negative potential energy differences relative to surrounding regions resulting in additional compressive stresses superimposed on the intraplate stresses derived from plate boundary forces – consistent with the dominance of reverse faulting earthquakes in the intraplate shield regions. Areas of high elevation and a thin mantle lid (e.g., western US Basin and Range, East African Rift, and Baikal Rift) are predicted to be in extension, consistent with the observed stress regime in these areas.

The simplicity of the observed crustal stress field thus appears most consistent with buoyancy-related forces acting directly on and within the lithosphere – in particular, ridge push and internal lithosphere density heterogeneities. Possible contributions from deep-mantle density heterogeneities, or tractions, from the flow they induce seem to be small or even unresolvable. More detailed stress data coverage and more accurate mantle/lithosphere models will be needed to determine the exact balance of forces, as well as the potential significance of drag forces. The body of work modeling stresses over the past 30 years seems to generally support the broad conclusions of the very first comprehensive modeling attempt by Richardson *et al.* (1979) – that ridge push and net slab pull (downwelling pull balanced by viscous and frictional resistance to subduction) were of comparable size and that shear tractions on the base of the plates are relatively small. As Richardson and Reding pointed out in 1981 in their modeling of stresses within the North American Plate, the large lateral gradients in stress magnitudes (up to an order of magnitude variation) across large plates, required by models in which drag dominates, are not observed.

6.06.4 Absolute Stress Magnitudes and the Critically Stressed Crust

Direct measurements of stress to depths of ~8 km have confirmed a simple yet profound model of how stress magnitudes vary with depth within the crust. This simple model is one of frictional faulting equilibrium or 'critically stressed crust' in which actual

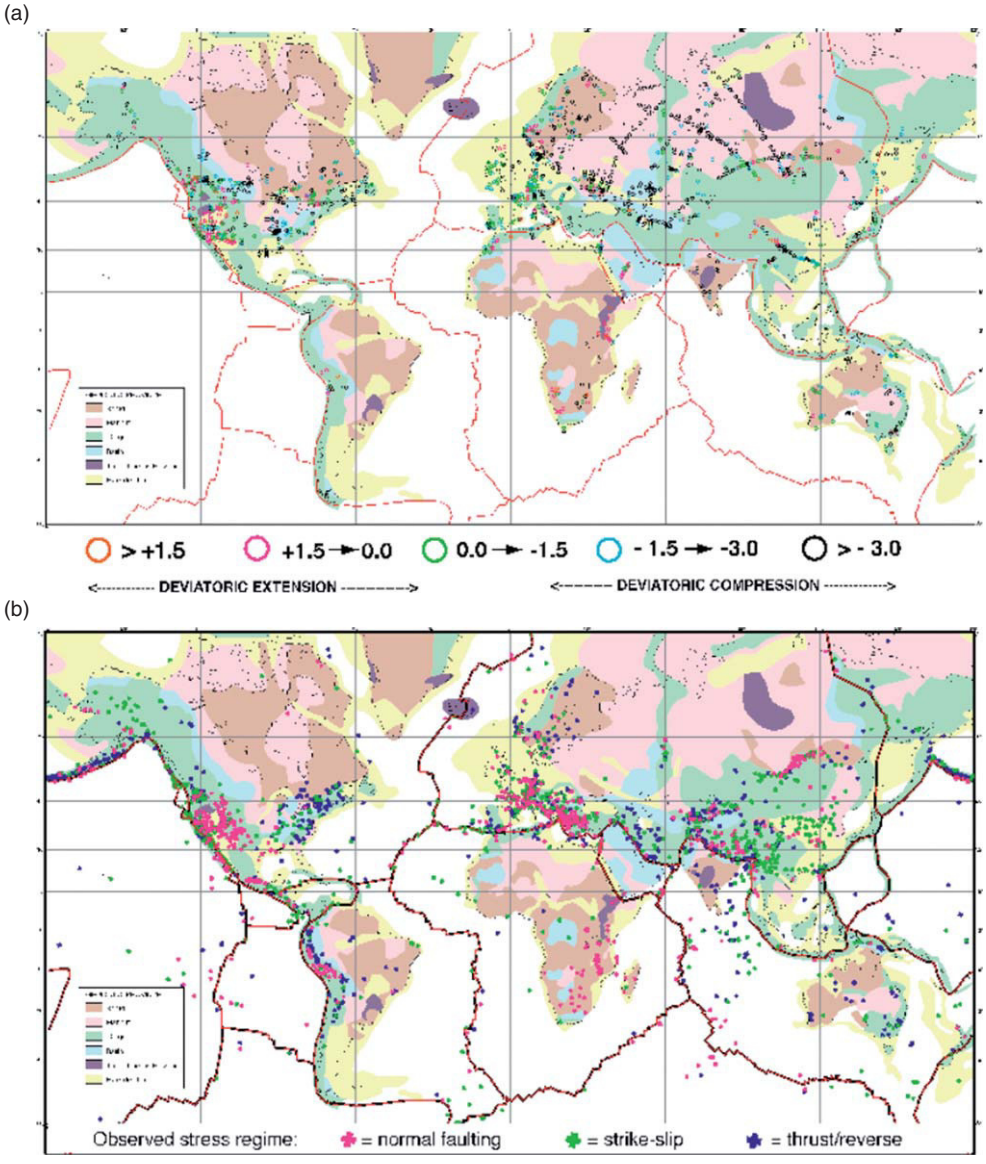

Figure 2 (a) Map of computed potential energy differences relative to a reference asthenosphere geoid shown on a base of tectonic provinces after Goodwin (1996). Positive potential energy differences giving rise to deviatoric extensional stresses are shown in red and magenta, weak negative potential energy differences are shown in green, and negative potential energy differences are shown in cyan and blue represent the largest deviatoric compression values implying strong deviatoric compressional stresses. (b) Observed stress regime data from the World Stress Map database. These represent a subset of the entire database and are those data points with stress regime information, primarily earthquake focal mechanisms and geologic stress indicators. Magenta indicates an extensional stress regime, characterized by normal faulting. Green shows data indicating strike-slip faulting. Blue points represent areas of a strongly compressional stress regime, characterized by thrust or reverse faulting. Reproduced from Zoback ML and Mooney WD (2003) Lithospheric buoyancy and continental intraplate stress. *International Geology Review* 45: 95–118, with permission from American Geophysical Union.

stress differences in the crust are very close to the values required for slip on the most well-oriented, preexisting faults. This model is based on classic Coulomb faulting theory and confirmed by laboratory tests of rock failure. It is also the basis for the linear portion of lithospheric strength curves first developed by Brace and Kohlstedt (1980) that show maximum stress differences (i.e., strength) as a function of depth; the integral of these stress-difference profiles yields lithospheric strength. As reviewed by Zoback *et al.*

(2002) and summarized below, the implications of a critically stressed crust are profound.

According to Coulomb theory, fault slippage will occur when the shear stress on the fault τ equals the sum of the inherent fault strength S_o and the frictional resistance to sliding (the product of μ, the coefficient of friction on the fault, and σ_n, the stress acting normal to the fault plane):

$$\tau = S_o + \mu\sigma_n \quad [4]$$

(cf., Jaeger and Cook, 1979). The maximum shear stress is given as $(S_1 - S_3)/2$ and corresponds to the most well-oriented fault planes for slip.

Actual stress magnitudes in the Earth's crust are modified by internal pore pressure in the rock. The concept of 'effective stress' is used to incorporate the influence of pore pressure at depth, a component of effective stress σ_{ij} is related to the total stress S_{ij} via

$$\sigma_{ij} = S_{ij} - \delta_{ij} P_p \quad [5]$$

where δ_{ij} is the Kronecker delta and P_p is the pore pressure.

By applying the concept of effective stress to Anderson faulting theory, we can predict stress magnitudes at depth for different stress regimes. Two-dimensional faulting theory assumes that failure on pre-existing faults is a function only of the difference between the least and greatest principal effective stresses σ_1 and σ_3. In this case, the ratio of stress magnitudes of σ_1 and σ_3 can be shown to be a constant, related to the frictional coefficient of the most favorably oriented faults:

$$\sigma_1/\sigma_3 = (S_1 - P_p)/(S_3 - P_p) = \left((\mu^2 + 1)^{1/2} + \mu\right)^2 \quad [6]$$

(after Jaeger and Cook, 1971). Since the coefficient of friction is relatively well defined for most rocks and ranges between ~0.6 and 1.0 (Byerlee, 1978), eqn [6] indicates that frictional sliding will occur when $\sigma_1/\sigma_3 \sim 3$.

Assuming hydrostatic pore pressure (a common assumption for which a complete justification is given later in this section) and that the vertical stress is equal to the weight of the overburden, we can compute absolute stress magnitudes for the three main Andersonian faulting regimes:

- normal faulting, extensional regimes: $S_{hmin} \sim 0.6\ S_v$,
- reverse faulting, compressional regimes: $S_{Hmax} \sim 2.3\ S_v$,
- strike-slip faulting regimes: (when $S_v \sim 1/2\ S_{Hmax} + S_{hmin}$), $S_{Hmax} \sim 2.2\ S_{hmin}$.

This simple model of crustal stress magnitude has been validated by a large number of *in situ* stress measurements in deep wells and scientific boreholes (see review by Townend and Zoback (2000)). The deepest and most complete set of stress magnitude data (collected to ~8 km depth in a scientific borehole in Germany) is shown in **Figure 3**. The measured stresses indicate a strike-slip stress regime and the stress differences throughout the entire depth range sampled are consistent with frictional faulting equilibrium with a frictional coefficient of ~0.7 (dashed line above 10 km) (Zoback *et al.*, 1993; Brudy *et al.*, 1997). Further evidence for such a 'frictional failure' stress state is provided by a series of earthquakes that were triggered at ~9 km

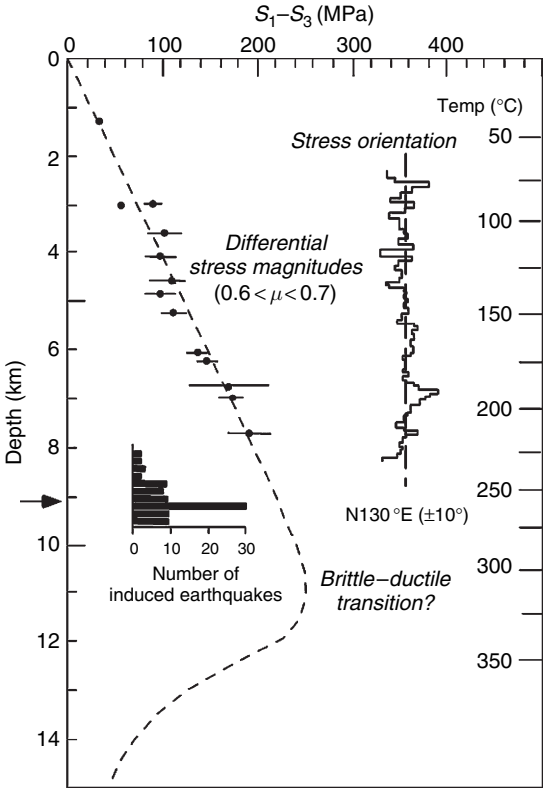

Figure 3 Stress measurements in the German scientific research well, KTB, indicate a strong crust, in a state of failure equilibrium as predicted by Coulomb theory and laboratory-derived coefficients of friction of 0.6–0.7. The arrow at 9.2 km depth indicates where the fluid injection experiment occurred. Reproduced from Zoback MD and Harjes HP (1997) 'Injection induced earthquakes and crustal stress at 9 km depth at the KTB deep drilling site, Germany.' *Journal of Geophysical Research* 102: 18477–18491, with permission from American Geophysical Union.

depth in rock surrounding the borehole with extremely low perturbations of the ambient, approximately hydrostatic pore pressure (Zoback and Harjes, 1997).

Figure 4 (from Zoback and Townend (2001) and Townend and Zoback (2000)) shows a compilation of stress measurements in relatively deep wells and boreholes from a variety of tectonic provinces around the world. As shown in **Figure 4(a)**, the ratio of the measured maximum and minimum effective stresses (as shown in eqn [6]) corresponds to values predicted from frictional faulting equilibrium with a coefficient of friction ranging between 0.6 and 1.0, the same range as that observed in the laboratory (Byerlee, 1978). Additional data collected at shallower depths in the crust (<3 km) substantiate the observation that the upper crust is critically stressed according to Mohr–Coulomb frictional failure theory (see reviews by McGarr and Gay (1978) and Zoback and Healy (1992)). **Figure 4(b)** shows the same stress measurement as presented in **Figure 3(a)** but this time as a function of apparent depth (see Townend and Zoback, 2000). As shown, stress magnitudes increase rapidly with depth in the brittle crust.

Two important implications of the data in **Figure 4** are worth noting. First, 'Byerlee's law' (i.e., that the coefficient of frictional sliding is in the range 0.6–1.0 in the brittle crust, independent of rock type) was defined on the basis of hundreds of laboratory experiments, yet it appears to correspond to faults *in situ* equally well. This is a surprising result given the large difference between the size of samples used for friction experiments in the laboratory, the size of real faults *in situ*, the variability of roughness of the sliding surface, and the idealized conditions under which laboratory experiments are conducted, etc. Second, despite the fact that Earth's brittle crust contains a spectrum of widely distributed faults, fractures, and planar discontinuities at many different scales and orientations, it appears that stress magnitudes at depth (specifically, the differences in magnitude between the maximum and minimum principal stresses) are limited by the frictional strength of the most well-oriented of these planar discontinuities.

Because frictional strength depends on pore pressure, it is important to note that the measured stress data shown in **Figure 4** are all associated with essentially hydrostatic pore pressures, suggestive of relatively high permeability throughout the upper crust. By analyzing the results of *in situ* hydraulic tests conducted at length scales of 10–1000 m and to depths as great as 9 km as well as the migration rates of induced seismicity over distances of up to several

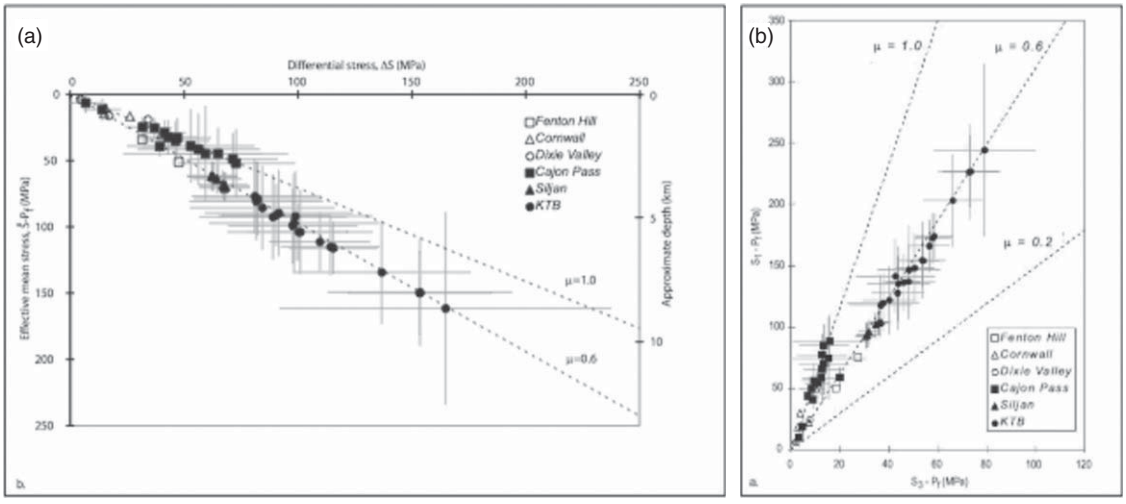

Figure 4 (a) *In situ* stress measurements in relatively deep wells in crystalline rock indicate that stress magnitudes seem to be controlled by the frictional strength of faults with coefficients of friction between 0.6 and 1.0. (b) When converted to approximate depth, the deep borehole stress measurements indicate a rapid increase in depth, as seen in lithospheric strength profiles. (a) Reproduced from Zoback MD and Townend J (2001) Implications of hydrostatic pore pressures and high crustal strength for the deformation of intraplate lithosphere. *Tectonophysics* 336: 19–30, with permission from American Geophysical Union. (b) Reproduced from Townend J and Zoback MD (2000) 'How faulting keeps the crust strong' *Geology* 28(5): 399–402, with permission from American Geophysical Union.

kilometers, Townend and Zoback (2000) inferred upper-crustal permeabilities between $\sim 10^{-17}$ and $10^{-16}\,m^2$, three to four orders magnitude higher than that of core samples studied in the laboratory at equivalent pressures. Geothermal and metamorphic data also indicate that the permeability of the upper crust is high ($>10^{-18}\,m^2$) throughout the brittle regime (Manning and Ingebritsen, 1999).

In fact, we believe that the mechanism responsible for creating and maintaining high crustal permeability is fundamentally related to the observation that the crust is in a state of frictional faulting equilibrium. Using data from several scientific boreholes, Barton *et al.* (1995) demonstrated that optimally oriented planes are hydraulically conductive, whereas nonoptimally oriented planes are nonconductive. This conclusion is supported by data collected subsequently from even deeper boreholes in other tectonic settings (Hickman *et al.*, 1997; Barton *et al.*, 1998) and the 8 km deep borehole in Germany (Ito and Zoback, 2000). Another way of saying this is that the active faults that limit crustal strength are also responsible for maintaining pore pressures at hydrostatic values. These results clearly indicate that critically stressed faults act as fluid conduits and control large-scale permeability (Townend and Zoback, 2000; Zoback and Townend, 2001). Thus, the presence of critically stressed faults in the crust keeps the brittle crust permeable and upper-crustal pore pressures close to hydrostatic values.

Three independent lines of evidence support the *in situ* measurements in indicating a critically stressed crust at frictional faulting equilibrium:

- the widespread occurrence of crustal seismicity induced by either reservoir impoundment or fluid injection (cf. Healy *et al.*, 1968; Raleigh *et al.*, 1972; Pine *et al.*, 1990; and Zoback and Harjes, 1997);
- earthquakes triggered by small stress changes ($\sim$0.1–0.3 MPa) associated with other earthquakes (cf. Stein *et al.*, 1992); and
- relatively small stress drops in crustal earthquakes (1–10 MPa) (Hanks, 1977) typically an order of magnitude smaller than expected stress differences at seismogenic depths (as shown in **Figure 4(b)**).

All these observations imply that the stress driving and released in earthquake faulting involves relatively small fluctuations around frictional faulting equilibrium values.

6.06.5 Stress Field Constraints on Lithospheric Deformation

It might seem surprising that the state of stress in the crust is generally in a state of incipient frictional failure, especially in relatively stable intraplate areas. A significant implication of this observation is that observed variations in rates of active lithospheric deformation must be directly linked to lithospheric strength, not to large variations in stress state. One of the strongest parameters controlling integrated lithospheric strength is Moho temperature, (e.g., England and Molnar, 1991). Using surface heat flow as a proxy for Moho temperature, we can observe the strong correlation between lithospheric strength and deformation rate by comparing a map of US heat flow (Blackwell and Steele, 1992; Blackwell *et al.*, 1991) with the US National Seismic Hazard Map (Frankel *et al.*, 2002; (**Figure 5**). The seismic hazard map is not directly a strain-rate map, it portrays shaking hazard, which is proportional to the rate of seismicity as well as the potential size of likely earthquakes in a region, so it too is a proxy. Nonetheless, it is clear that in general within the regions of warmest crust are those deforming most rapidly.

The reason for the correlation between lithospheric strength and rate of deformation can be visualized in terms of a simple conceptual model of deforming lithosphere that is in balance with the forces acting on it. The lithosphere is generally represented as three distinct layers – brittle upper crust, ductile lower crust, and ductile uppermost mantle (**Figure 6**, from Zoback and Townend (2001) following previous workers). Deformation in the ductile lower crust and upper mantle is governed by power-law creep law (e.g., Brace and Kohlstedt, 1980). Because any applied force to the lithosphere will result in steady-state creep in the lower crust and upper mantle, as long as the 'three-layer' lithosphere is coupled, stress will build up in the upper brittle layer due to the creep at deeper levels. Stress in the upper crust builds over time, eventually to the point of brittle failure. The fact that intraplate earthquakes are relatively infrequent results simply from the fact that the rate of ductile strain rate is low in the lower crust and upper mantle (Zoback *et al.*, 2002).

The detailed manner in which stress in the lithosphere is related to deformation and deformation rate can be investigated using lithospheric strength

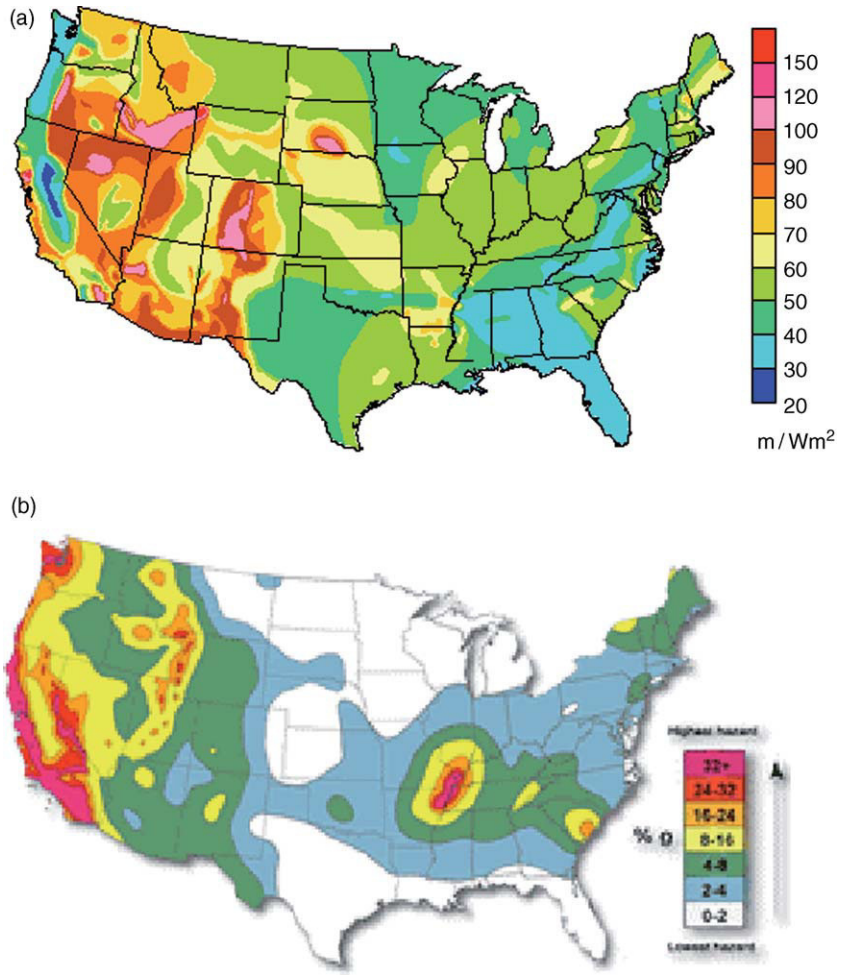

Figure 5 Comparison of (a) US heat flow (from Blackwell and Steele, 1992) with (b) the US National Seismic Hazard map (Frankel *et al.*, 2003). Note the strong correlation between regions high crustal temperature and regions of high deformation rate as indicated by high seismic hazard.

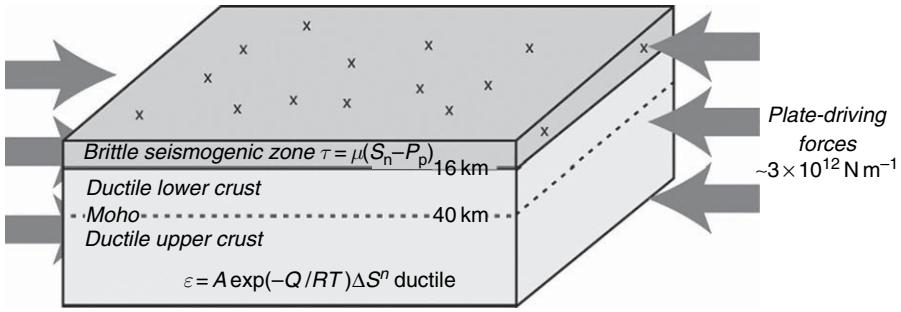

Figure 6 Schematic illustration of how the forces acting on the lithosphere keep the brittle crust in frictional equilibrium through creep in the lower crust and upper mantle. Reproduced from Zoback MD and Townend J (2001) Implications of hydrostatic pore pressures and high crustal strength for the deformation of intraplate lithosphere. *Tectonophysics* 336: 19–30, with permission from American Geophysical Union.

envelopes that incorporate brittle strength (based on frictional faulting equilibrium) and power-law creep with appropriate rheologies to represent the ductile behavior. Depending on thermal regime, there may be zones of brittle deformation in the lower crust and upper mantle as well as the upper crust, if the stress

differences for brittle deformation are lower than those required for ductile deformation. Integrating this differential stress profile over the thickness of the lithosphere gives the cumulative strength (or force/length in these 2-D models) of the lithosphere.

Typically, investigators select a strain rate for the lithosphere and compute the total strength (force/length) required to deform the lithosphere at that rate (e.g., Sibson, 1983; Ranalli and Murphy, 1987; Kohlstedt *et al.*, 1995). Zoback and Townend (2001) proposed an alternate approach to modeling lithospheric deformation by assuming a value for the cumulative force deforming the lithosphere and then calculating the resulting strain rate as a function of temperature and rheology. They applied this force-limited, steady-state deformation model to two end-member intraplate regions that differ markedly in their average surface heat flow, but with identical lithosphere structures – both have a 40 km-thick crust and a 60-km-thick mantle lid (**Figure 7**). The temperature profiles in **Figure 7** were computed assuming simple heat productivity models and downward continuation of surface heat flow and allowing thermal conductivity to be a function of both temperature and depth. A strike-slip/reverse faulting stress state (i.e., $S_1 > S_2 > S_3 \sim S_v$) was also assumed, consistent with the general compressional state of stress observed in most mid-plate and intraplate regions (see Zoback (1992)). Pore pressures in the lower crust were assumed to be near-lithostatic, following the arguments presented by Nur and Walder (1990) and consistent with the

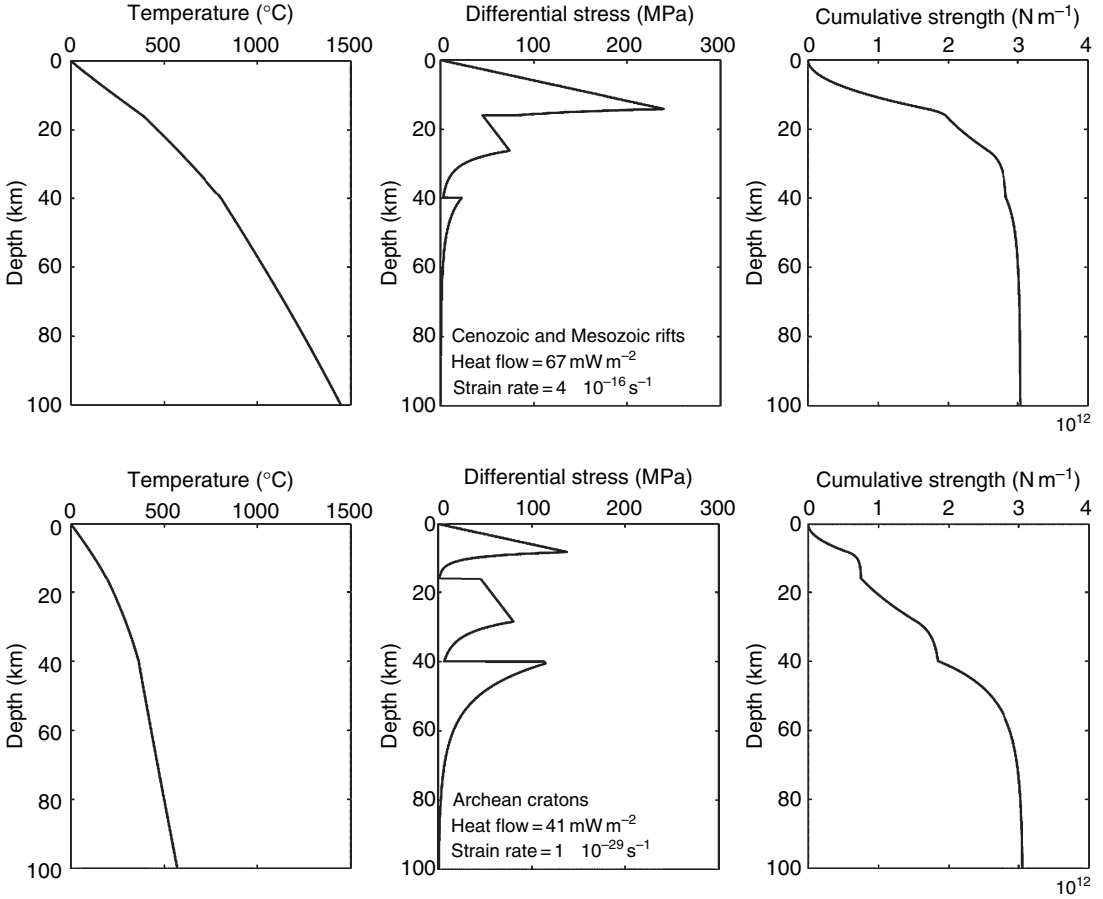

Figure 7 A comparison between theoretical temperature, differential stress, and cumulative strength profiles for two representative intraplate regions, an area of moderate heat flow (67 m W m^{-2}) and a shield area with very low heat flow (41 mW m^{-2}). As detailed in Zoback and Townend (2001) a lithospheric structure composed of a 16-km-thick felsic upper crust (with the rheological properties of dry Adirondack granulite), a 24-km-thick mafic lower crust (dry Pikwitonei granulite), and a 60-km-thick lithospheric mantle (wet Aheim dunite) assumed. Reproduced from Zoback MD, Townend J, and Grollimund B (2002) Steady-state failure equilibrium and deformation of intraplate lithosphere. *International Geology Review* 44: 383–401, with permission from American Geophysical Union.

conclusions of Manning and Ingebritsen (1999) that permeability of the lower crust probably does not exceed $10^{-19}\,m^2$ at 30 km depth implying relatively long characteristic diffusion times (>10^5years) consistent with maintaining near-lithostatic pore pressures.

Using the temperature–depth profiles shown in **Figure 7**, Zoback and Townend calculated differential stresses in the ductile portion of the upper and lower crust and lithospheric mantle and the corresponding ductile strain rate, such that the cumulative area under the stress profile (lithospheric strength) does not exceed the assumed total force/length available to deform the lithosphere, $\sim 3 \times 10^{12}\,N\,m^{-1}$. The rationale for limiting the deforming force/length to this value is based on the extensive stress modeling summarized in the previous section indicating that the magnitude of the cumulative forces acting on the lithosphere are generally on the order of the ridge push force, which is fairly well constrained between $1–5 \times 10^{12}\,N\,m^{-1}$ based on oceanic crust and lithosphere density and structure data.

The more than 12 orders of magnitude difference in the computed strain rates between the two regions subjected to the same force/length is thus related to their relative strengths. As seen in the upper half of **Figure 7**, a situation representative of intraplate Cenozoic and Mesozoic rifted crust with moderately high heat flow ($\sim 67\,mW\,m^{-2}$) exhibits relatively high strain rates ($\sim 10^{-16}\,s^{-1}$). This is due to the relatively high temperatures in the lower crust and upper mantle, so that relatively little force is required to cause deformation there. Note too that in this case, most of the total tectonic force is carried in the strong brittle crust. On geologic timescales this region would appear to deform as a viscous continuum.

In contrast, in a cold shield region (lower half of **Figure 7**) the lower crust and upper mantle are considerably stronger and the total force available is sufficient to only strain the lithosphere at a rate of $\sim 10^{-29}\,s^{-1}$, a negligible rate (even over billions of years!) and thus consistent with a rigid plate assumption. Differences in strength of the two regions are largely driven by the >400 K difference in temperature at the Moho (40 km depth) (**Figure 7**).

A test of such a force-limited, steady-state model is that the estimated intraplate lithospheric strain rates not exceed approximately $10^{-17}\,s^{-1}$, in order to be consistent with plate tectonic reconstructions assuming 'rigid' plates (e.g., Gordon, 1998). Because calculations such as those in **Figure 7** involve a large number of parameters (surface heat flow, thermal conductivity, upper-crustal heat productivity, the frictional coefficient of the crust and the rheological parameters of each layer), Zoback and Townend (2001) treated uncertainties in each of these parameters using a Monte Carlo technique: 1000 estimates of each parameter were drawn at random from normal distributions, and 1000 separate models were constructed. Composite temperature–depth, differential stress–depth, and strength–depth profiles were then constructed by stacking the different models' results.

Figure 8 illustrates the intraplate lithosphere modeling results for surface heat flow of $60 \pm 6\,mW\,m^{-2}$ (mean ± 10%), representative of stable continental heat flow (Pollack *et al.*, 1993). The uppermost plots (**Figure 8(a)–8(c)**) display the model results incorporating hydrostatic pore pressures in the upper crust, and the three middle plots (**Figure 8(d)–8(f)**) display the corresponding results for near-lithostatic pore pressures. Note that the temperature–depth profiles are the same in both cases. At the bottom of **Figure 8** is a histogram (**Figure 8(g)**) illustrating the range of estimated strain rates under each pore pressure condition: the strain rates are distributed log-normally about a geometric mean of approximately $10^{-18}\,s^{-1}$ under 'near-hydrostatic upper-crustal pore-pressure' conditions, and approximately $10^{-15}\,s^{-1}$ for near-lithostatic pore-pressure conditions. This latter value is much too high to be consistent with geologic and geodetic observations, and demonstrates the importance of near-hydrostatic fluid pressures in the upper crust for maintaining the strength of intraplate lithosphere. Although we do not illustrate it here, it is important to note that for very low surface heat flow ($<50 \pm 5\,mW\,m^{-2}$) such as is characteristic of Proterozoic and Archean cratonic crust (Pollack *et al.*, 1993), strain rates lower than $10^{-20}\,s^{-1}$ are expected under either pore-pressure regime.

Thus, at the relatively low strain rates characterizing intraplate regions, there is sufficient plate-driving force available to overcome the integrated strength of the lithosphere, causing ductile deformation and maintaining the 'strong' brittle crust in a state of frictional failure equilibrium. One manifestation of high crustal strength is the efficient transmission of tectonic stress over distances of thousands of kilometers in intraplate regions documented by the stress orientation and relative magnitude data. Thus, in essence, upper crust acts as a very efficient stress guide.

As an example of how lithospheric strength variations concentrate deformation, consider the partition of deformation along the San Andreas Fault System

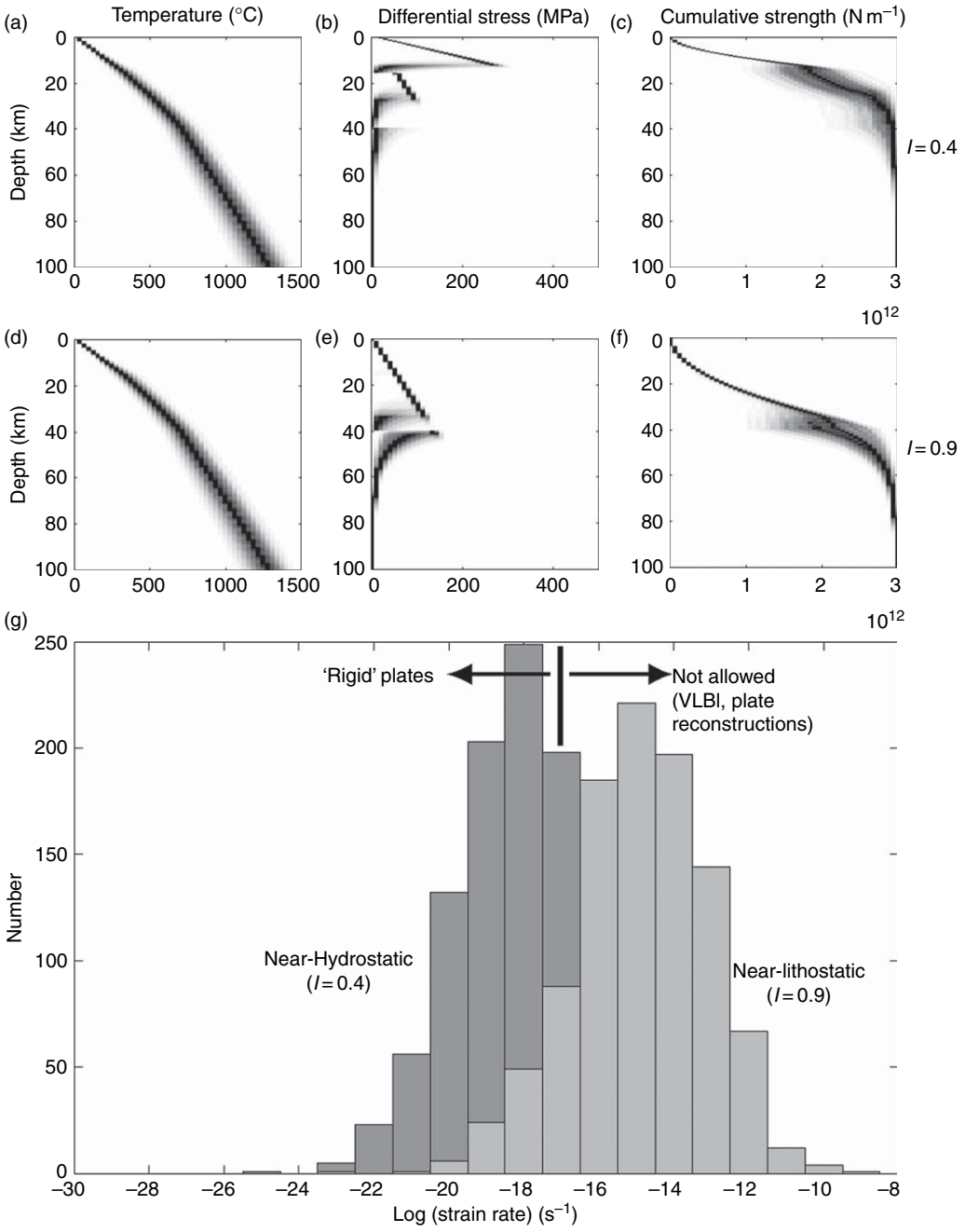

Figure 8 (a–g) Results of 1000 Monte Carlo strain rate calculations for a strike-slip stress state and surface heat flow of $60 \pm 6\,\mathrm{mW\,m^{-2}}$, subject to the constraint that the total strength of the lithosphere is $3 \times 10^{12}\,\mathrm{N\,m^{-1}}$. Reproduced from Zoback MD and Townend J (2001) Implications of hydrostatic pore pressures and high crustal strength for the deformation of intraplate lithosphere. *Tectonophysics* 336: 19–30, with permission from American Geophysical Union.

in central California. As pointed out by Page *et al.* (1998), deformation along the San Andreas system is transpressional; in addition to the right-lateral shear accommodating relative motion between the Pacific and North American Plates, appreciable fault-normal convergence has been occurring since about 3.5 Ma. This convergence has resulted in uplift, folding, and reverse faulting over a broad zone about 100 km wide and corresponding to the Coast Ranges adjacent to the San Andreas.

This type of distributed deformation could be categorized as a diffuse plate boundary (e.g., Gordon, 1998; Wessel and Mueller, 2007), but it is interesting to consider more specifically why the transpressional deformation is distributed so broadly, and why there is such an abrupt cessation of this deformation at the eastern boundary between the Coast Ranges and the Great Valley. The sharpness of this transition is particularly distinctive given that the entire region is subject to a relatively uniform compressive stress field acting at a high angle to the San Andreas Fault and subparallel strike-slip faults (**Figure 9**). This high angle implies that the San Andreas Fault (and perhaps other plate boundaries) have low frictional strength, in marked contrast to the high frictional strength exhibited by intraplate faults (briefly summarized by Zoback (2000)).

The stress observations shown in **Figure 9** (primarily from wellbore breakout measurements in oil and gas wells and earthquake focal mechanisms not associated with right-lateral slip along transform faults; see Mount and Suppe (1987) and Zoback *et al.* (1987)) are remarkably consistent with modeled stress directions across the region and shown by dashed trajectories, interpolated from the results of Flesch *et al.* (2000). As previously discussed, the Flesch *et al.* model incorporates the combined effects of buoyancy-related stresses in the western United States (principally due to the thermally uplifted Basin and Range Province) and right-lateral shear in the far field associated with plate interaction.

The abrupt changè in the rate of deformation at the eastern boundary between the Coast Ranges and Great Valley coincides with a marked decrease in heat flow, and therefore with lower-crustal and upper-mantle temperatures. Zoback *et al.* (2002) thus inferred that the rate of deformation is high throughout the Coast Ranges because temperatures in the lower crust and upper mantle are high. In contrast, heat flow in the Great Valley is extremely low (comparable to that of shield areas); hence, the available force is insufficient to cause deformation at appreciable rates. In fact, as revealed by undeformed seismic reflectors corresponding to formations as old as Cretaceous in age, it is remarkable how little deformation has occurred in the Great Valley during the Cenozoic (e.g., Wentworth and Zoback, 1989).

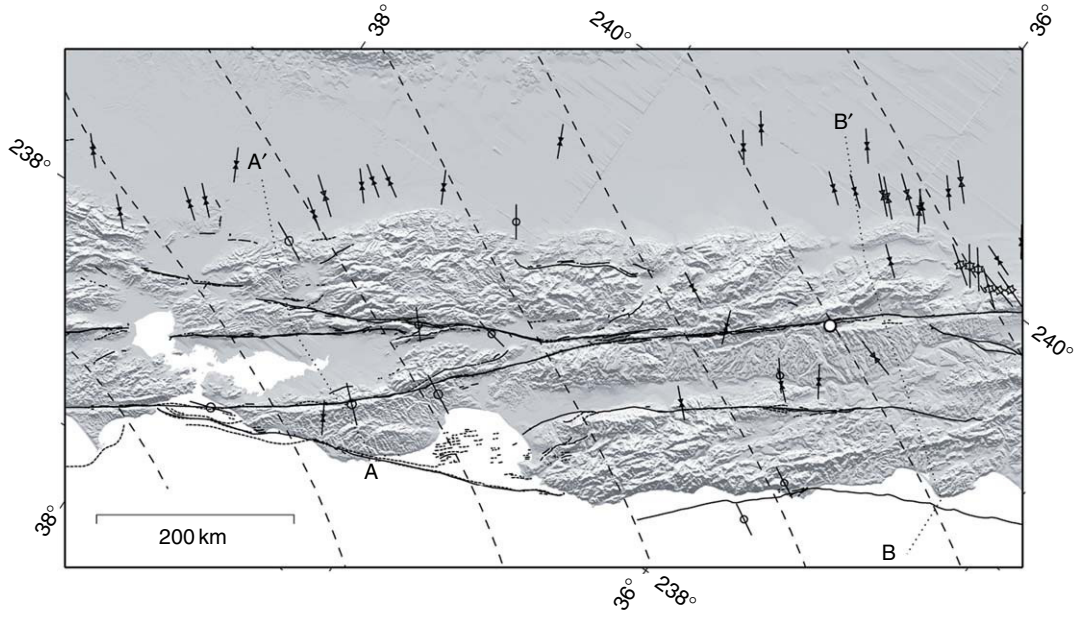

Figure 9 Topographic map of western California in an oblique Mercator projection about the NUVEL 1A North America–Pacific Euler pole (DeMets *et al.*, 1990). In this projection, relative plate motion is parallel to the upper and lower margins of the map. The major right-lateral strike-slip faults comprising the San Andreas Fault System are also shown. The data show the direction of maximum horizontal stress from earthquake focal mechanism inversions (lines with a circle in the middle) or borehole stress measurements (bow-tie symbols). The dashed trajectories are interpolations of stress directions calculated by Flesch *et al.* (2000) using a model based on lithospheric buoyancy and plate interaction. Reproduced from Townend and Zoback MD (2004), with permission from American Geophysical Union.

6.06.6 Concluding Remarks

Several decades of study have produced a surprisingly simple and consistent picture of the lithospheric state of stress:

- The lithospheric stress field is the result of present-day active tectonics, and not related to residual stresses from past tectonic activity – this is indicated by remarkably uniform stress orientations over broad regions of the lithosphere (scales up to thousands of kilometers) including consistency across major bends in old orogenic belts.
- The same forces acting on and within the plates to drive plate motion are largely responsible for the stress state within the plates – this is demonstrated by the consistency of broad regional intraplate stress field with stresses predicted by models of these driving forces. Buoyancy forces due to lateral variations in lithospheric structure and density are also a significant contributor to the intraplate stress field. Most regions of intraplate extension are in regions of high topography generated by a thinned mantle lid.
- Direct stress measurements to depths of 8.1 km in deep wells and scientific research boreholes confirm the fact that stress magnitudes within the brittle crust are controlled by frictional strength. In fact, stress differences within the upper brittle layer indicate a state of incipient frictional failure on well-oriented pre-existing fault planes.
- Because the brittle crust appears to be in a state of incipient frictional failure, the rate of deformation in a region is determined by the overall strength of the lithosphere, hence young, hot lithosphere (e.g., along active plate boundaries) deforms much more rapidly than colder, stronger lithosphere in mid-plate regions. However, measured stress magnitudes in the two contrasting tectonic regions would be identical.
- Balancing observed rates of lithospheric deformation with applied forces suggests that most of the stress within the lithosphere is carried in its strong, uppermost brittle crustal layer (from the surface to ~15–20 km depth).

Appendix 1: Indicators of Contemporary Stress

Zoback and Zoback (1980) developed an integrated stress mapping strategy in the lithosphere based on data from a variety of sources: earthquake focal plane mechanisms, young geologic data on fault slip and volcanic alignments, *in situ* stress measurements, and stress-induced wellbore breakouts, and drilling-induced tensile fractures. Each stress indicator is explained briefly below.

Earthquake Focal Mechanisms

While earthquake focal plane mechanisms are the most ubiquitous indicator of stress in the lithosphere, determination of principal stress orientations and relative magnitudes from these mechanisms must be done with appreciable caution. The pattern of seismic radiation from the focus of an earthquake permits construction of earthquake focal mechanisms. Perhaps the most simple and straightforward information about *in situ* stress that is obtainable from focal mechanisms and *in situ* stress is that the type of earthquake (i.e., normal, strike-slip, or reverse faulting) defines the relative magnitudes of S_{Hmax}, S_{hmin}, and S_v. In addition, the orientation of the fault plane and auxiliary plane (which bound the compressional and extensional quadrants of the focal plane mechanism) define the orientation of the P (compressional), B (intermediate), and T (extensional) axes. These axes are sometimes incorrectly assumed to be the same as the orientation of S_1, S_2, and S_3.

For cases in which laboratory-measured coefficients of fault friction of ~0.6–1.0 are applicable to the crust, there is usually not a large error if one uses the P, B, and T axes as approximations of average principal stress orientations, especially if the orientation of the fault plane upon which the earthquake occurred is known (Raleigh *et al.*, 1972). However, if friction is negligible on the faults in question, there can be considerable difference between the P, B, and T axes and principal stress directions (McKenzie, 1969). An earthquake focal plane mechanism always has the P and T axes at 45° to the fault plane and the B axes in the plane of the fault. With a frictionless fault the seismic radiation pattern is controlled by the orientation of the fault plane and not the *in situ* stress field. One result of this is that just knowing the orientation of the P-axis of earthquakes along weak, plate-bounding strike-slip faults (like the San Andreas) does not allow one to define principal stress orientations from the focal plane mechanisms of the strike-slip earthquakes occurring on the fault (Zoback *et al.*, 1987).

Principal stress directions can be determined directly from a group of earthquake focal mechanisms (or set of fault striae measurements) through use of inversion techniques that are based on the slip kinematics and the assumption that fault slip will

always occur in the direction of maximum resolved shear stress on a fault plane (cf., Angelier, 1990; Gephart and Forsyth, 1984; Michael, 1984). Such inversions yield four parameters, the orientation of the three principal stresses and the relative magnitude of the intermediate principal stress with respect to the maximum and minimum principal stress.

The analysis of seismic waves radiating from an earthquake also can be used to estimate the magnitude of stress released in an earthquake (stress drop), although not absolute stress levels (Brune, 1970). In general, stress drops of crustal earthquakes are on the order of 1–10 MPa (Hanks, 1977). Equation (7) can be used to show that such stress drops are only a small fraction of the shear stresses that actually cause fault slip if pore pressures are approximately hydrostatic at depth and Coulomb faulting theory (with laboratory-derived coefficients of friction) is applicable to faults *in situ*. This is discussed in more detail below.

Geologic Stress Indicators

There are two general types of 'relatively young' geologic data that can be used for *in situ* stress determinations: (1) the orientation of igneous dikes or cinder cone alignments, both of which form in a plane normal to the least principal stress (Nakamura, 1977) and (2) fault slip data, particularly the inversion of sets of striae (i.e., slickensides) on faults as described above. Of course, the term 'relatively young' is quite subjective but essentially means that the features in question are characteristic of the tectonic processes currently active in the region of question. In most cases, the WSM database utilizes data which are Quaternary in age, but in all areas represent the youngest episode of deformation in an area.

In Situ stress Measurements

Numerous techniques have been developed for measuring stress at depth. Amadei and Stephansson (1997) and Engelder (1993) discuss many of these stress measurement methods, most of which are used in mining and civil engineering. Because we are principally interested here in regional tectonic stresses (and their implications) and because a variety of nontectonic processes affect *in situ* stresses near the earth's surface (Engelder and Sbar, 1984), we do not utilize near-surface stress measurements in the WSM or regional tectonic stress compilations (these measurements are given the lowest quality in the criteria used by WSM since they are not believed to be reliably indicative of the regional stress). In general, we believe that only *in situ* stress measurements made at depths greater than 100 m are indicative of the tectonic stress field at mid-crustal depths. This means that techniques utilized in wells and boreholes, which access the crust at appreciable depth, are especially useful for stress measurements.

When a well or borehole is drilled, the stresses that were previously supported by the exhumed material are transferred to the region surrounding the hole. The resultant stress concentration is well understood from elastic theory. Because this stress concentration amplifies the stress difference between far-field principal stresses by a factor of 4, there are several other ways in which the stress concentration around boreholes can be exploited to help measure *in situ* stresses. The hydraulic fracturing technique (e.g., Haimson and Fairhurst, 1970; Zoback and Haimson, 1982) takes advantage of this stress concentration and, under ideal circumstances, enables stress magnitude and orientation measurements to be made to about 3 km depth (Baumgärtner *et al.*, 1990).

The most common method of determining stress orientation from observations in wells and boreholes are stress-induced wellbore breakouts. Breakouts are related to a natural compressive failure process that occurs when the maximum hoop stress around the hole is large enough to exceed the strength of the rock. This causes the rock around a portion of the wellbore to fail in compression (Bell and Gough, 1979; Zoback *et al.*, 1985). For the simple case of a vertical well drilled when S_v is a principal stress, this leads to the occurrence of stress-induced borehole breakouts that form at the azimuth of the minimum horizontal compressive stress. Breakouts are an important source of crustal stress information because they are ubiquitous in oil and gas wells drilled around the world and because they also permit stress orientations to be determined over a great range of depth in an individual well. Detailed studies have shown that these orientations are quite uniform with depth, and independent of lithology and age (e.g., Castillo and Zoback, 1994).

Another form of naturally occurring wellbore failure is drilling-induced tensile fractures. These fractures form in the wall of the borehole at the azimuth of the maximum horizontal compressive stress when the circumferential stress acting around the well locally goes into tension, they are not seen in core from the same depth (Moos and Zoback, 1990; Brudy and Zoback, 1993, 1999; Brudy *et al.*, 1997; Lund and Zoback, 1999; Peska and Zoback, 1995).

References

Amadei B and Stephansson O (1997) *Rock Stress and Its Measurement*. London: Chapman and Hall.

Anderson EM (1951) *The Dynamics of Faulting and Dyke Formation with Applications to Britain*, 206 pp. Edinburgh: Oliver and Boyd.

Angelier J (1979) 'Determination of the mean principal directions of stresses for a given fault population.' *Tectonophysics* 56: T17–T26.

Angelier J (1984) 'Tectonic analysis of fault slip data sets.' *Journal of Geophysical Research* 89: 5835–5848.

Artyushkov EV (1973) Stresses in the lithosphere caused by crustal thickness inhomogeneities. *Journal of Geophysical Research* 78: 7675–7708.

Bai W, Vigny C, Ricard Y, and Froidevaux C (1992) On the origin of deviatoric stresses in the lithosphere. *Journal of Geophysical Research* 97: 11729–11737.

Barton CA, Zoback MD, and Moos D (1995) 'Fluid flow along potentially active faults in crystalline rock.' *Geology* 23: 683–686.

Barton CA, Hickman SH, Morin R, Zoback MD, and Benoit D (1998) Reservoir-scale fracture permeability in the Dixie Valley, Nevada, geothermal field: Abstracts Volume, Society of Petroleum Engineers Annual Meeting, Trondheim, Paper Number 47371, p. 315–322.

Baumgärtner J, Rummel F, Zoback MD (1990) Hydraulic fracturing *in situ* stress measurements to 3 km depth in the KTB pilot hole VB. A summary of a preliminary data evaluation, in KTB Report 90–6a: 353–400.

Bell JS and Gough DI (1979) Northeast–southwest compressive stress in Alberta: Evidence from oil wells. *Earth and Planetary Science Letters* 45: 475–482.

Bird P (1998) Testing hypotheses on plate-driving mechanisms with global lithosphere models including topography, thermal structure and faults. *Journal of Geophysical Research* 103: 10115–10129.

Brace WF and Kohlstedt DL (1980) Limits on lithospheric stress imposed by laboratory experiments. *Journal of Geophysical Research* 85: 6248–6252.

Blackwell DD and Steele JL (1992) Geothermal Map of North America. Geological Society of America DNAG Map No. 006.

Blackwell DD, Steele JL, and Carter LS (1991) Heat flow patterns of the North American continent: A discussion of the DNAG geothermal map of North America. In: Slemmons DB, Engdahl ER, and Blackwell DD (eds.) *Neotectonics of North America: Geological Society of America DNAG Decade Map,* vol. 1, pp. 423–437 (498pp.). Boulder, CO: Geological Society of America.

Brudy M and Zoback MD (1993) 'Compressive and tensile failure of boreholes arbitrarily-inclined to principal stress axes: Application to the KTB boreholes, Germany.' *International Journal Rock Mechanics Mining Sciences* 30: 1035–1038.

Brudy M and Zoback MD (1999) 'Drilling-induced tensile wall-fractures: Implications for the determination of *in-situ* stress orientation and magnitude.' *International Journal of Rock Mechanics and Mining Sciences* 36: 191–215.

Brudy M, Zoback MD, Fuchs K, Rummel F, and Baumgärtner J (1997) 'Estimation of the complete stress tensor to 8 km depth in the KTB scientific drill holes: Implications for crustal strength.' *Journal of Geophysical Research* 102: 18453–18475.

Brune JN (1970) Tectonic stress and the spectra of seismic shear from earthquakes. *Journal of Geophysical Research* 75: 4997–5009.

Byerlee JD (1978) Friction of rock. *Pure and Applied Geophysics* 116: 615–626.

Castillo D and Zoback MD (1995) 'Systematic stress variations in the Southern San Joaquin valley and along the White Wolf fault: Implications for the rupture mechanics of the 1952 Ms 7.8 Kern County earthquake and contemporary seismicity.' *Journal of Geophysical Research* 100(B4): 6249–6264.

Castillo DA and Zoback MD (1994) Systematic variations in stress state in the Southern San Joaquin Valley: Inferences based on well-bore data and contemporary seismicity. *American Association Petroleum Geologists Bulletin* 78(8): 1257–1275.

Chapple WM and Tullis TE (1977) Evaluation of the forces that drive the plates. *Journal of Geophysical Research* 82: 1967–1984.

Cloetingh SAPL and Wortel MJR (1985) Regional stress field of the Indian Plate. *Geophysical Research Letters* 12: 77–80.

Cloetingh SAPL and Wortel MJR (1986) Stress in the Indo-Australian plate. *Tectonophys* 132: 49–67.

Coblentz DD and Richardson RM (1996) Analysis of the South American intraplate stress field. *Journal of Geophysical Research* 101: 8643–8657.

Coblentz DD, Richardson RM, and Sandiford M (1994) On the gravitational potential of the Earth's lithosphere. *Tectonics* 13: 929–945.

Coblentz DD and Sandiford M (1994) Tectonic stresses in the African plate: Constraints on the ambient lithospheric stress state. *Geology* 22: 831–834.

Coblentz DD, Zhou S, Hillis RR, Richardson RM, and Sandiford M (1998) Topography, boundary forces, and the Indo-Australian intraplate stress field. *Journal of Geophysical Research* 103: 919–931.

Colmenares LB and Zoback MD (2003) stress field and seismotectonics of Northern South America. *Geology* 31: 721–724.

DeMets C, Gordon RG, Argus DF, and Stein S (1990) Current plate motions. *Geophysical Journal International* 101: 425–478.

Engelder T (1993) *Stress Regimes in the Lithosphere*. Princeton, New Jersey: Princeton University Press.

Engelder T and Sbar ML (1984) Near-surface *in situ* stress: Introduction. *Journal of Geophysical Research* 89: 9321–9322.

England PC and Molnar P (1991) Inferences of deviatoric stress in actively deforming belts from simple physical models. *Philosophical Transactions of the Royal Society of London, A* 337: 73–81.

Fleitout L (1991) The sources of lithospheric tectonic stresses. *Philosophical Transactions of the Royal Society of London Series A* 337: 73–81.

Fleitout L and Froidevaux C (1982) Tectonics and topography for a lithosphere containing density heterogeneities. *Tectonics* 1: 21–56.

Fleitout L and Froidevaux C (1983) Tectonic stresses in the lithosphere. *Tectonics* 2: 315–324.

Flesch LM, Holt WE, Haines AJ, and Shen-Tu B (2000) Dynamics of the Pacific-North American plate boundary in the Western United States. *Science* 287: 834–836.

Frankel AD, Petersen MD, Mueller CS, *et al.* (2002) Documentation for the 2002 Update of the National Seismic Hazard Maps: USGS Open-File Report 02-420, 33pp.

Forsyth DW and Uyeda S (1975) On the relative importance of driving forces of plate motion. *Geophysical Journal of the Royal Astronomical Society* 43: 163–200.

Gephart JW and Forsyth DW (1984) 'An improved method for determining the regional stress tensor using earthquake focal mechanism data: Application to the San Fernando earthquake sequence.' *Journal of Geophysical Research* 89: 9305–9320.

Goodwin AM (1996) *Principles of Precambrian Geology*, 327 pp. London: Academic Press.

Gordon RG (1998) The plate tectonic approximation: Plate nonrigidity, diffuse plate boundaries, and global plate reconstructions. *Annual Review of Earth and Planetary Sciences* 26: 615–642.

Govers R and Meijer PT (2001) On the dynamics of the Juan de Fuca plate. *Earth and Planetary Science Letters* 189: 115–131.

Grand S, van der Hilst RD, and Widiyantoro S (1997) Global seismic tomography: A snapshot of convection in the Earth. *GSA Today* 7: 1–7.

Grollimund BR and Zoback MD (2001) 'Impact of glacially-induced stress changes on hydrocarbon exploration offshore Norway.' *American Association of Petroleum Geologists Bulletin* 87(3): 493–506.

Grunthal G and Stromeyer D (1992) The recent crustal stress field in central Europe – Trajectories and finite-element modeling. *Journal of Geophysical Research* 97: 11805–11820.

Haimson BC and Fairhurst C (1970) *In situ* stress determination at great depth by means of hydraulic fracturing. In: Sumerton W (ed.) *Proceedings of the 11th US Symposium on Rock Mechanics*, pp. 559–584. New York: Society of Mining Engineers of AIME.

Hanks TC (1977) Earthquake stress drops, ambient tectonic stresses and stresses that drive plate motions. *Pure and Applied Geophysics* 115: 441–458.

Healy JH, Rubey WW, Griggs DT, and Ralieg CB (1968) 'The Denver earthquakes.' *Science* 161: 1301–1310.

Hickman SH, Barton CA, Zoback MD, Morin R, Sass J, and Benoit R (1997) '*In-situ* stress and fracture permeability along the Stillwater fault zone, Dixie Valley, Nevada.' *International Journal of Rock Mechanics and Mining Sciences* 34: 3–4 (Paper No. 126).

Hildenbrand TG (1985) Rift Structure of the Northern Mississippi Embayment from the analysis of gravity and magnetic data. *Journal of Geophysical Research* 90: 12607–12622.

Ito T, Zoback MD, and Peska P (2001) 'Utilization of mud weights in excess of the least principal stress to stabilize wellbores: Theory and practical examples.' *Society of Petroleum Engineers Drilling and Completions* 16: 221–229.

James TS and Bent AL (1994) A comparison of Eastern North American seismic strain-rates to glacial rebound strain-rates. *Geophysical Research Letters* 21: 2127–2130.

Jones CH, Unruh JR, and Sonder LJ (1996) The role of gravitational potential energy in active deformation in the Southwestern United States. *Nature* 381: 37–41.

Kohlstedt DL, Evans B, and Mackwell SJ (1995) Strength of the lithosphere: Constraints imposed by laboratory experiments. *Journal of Geophysical Research* 100: 17587–17602.

Lachenbruch AH, Sass JH, and Galanis SP, Jr. (1985) Heat flow in southernmost California and the origin of the Salton Trough. *Journal of Geophysical Research* 90: 6709–6736.

Lachenbruch AH and Morgan P (1990) Continental extension, magmatism and elevation; formal relations and rules of thumb. *Tectonophysics* 174: 39–62.

Lithgow-Bertelloni C and Guynn JH (2004) Origin of the lithospheric stress field. *Journal of Geophysical Research* 109: B01408 (doi: 10.1029/2003JB002467).

Lund B and Zoback MD (1999) Orientation and magnitude of *in situ* stress to 6.5 km depth in the Baltic Shield. *International Journal of Rock Mechanics and Mining Sciences* 36: 169–190.

Manning CE and Ingebritsen SE (1999) Permeability of the continental crust: Implications of geothermal data and metamorphic systems. *Reviews of Geophysics* 37: 127–150.

Meijer PT, Govers R, and Wortel MJR (1997) Forces controlling the present-day state of stress of the Andes. *Earth and Planetary Science Letters* 148: 157–170.

Meijer PT and Wortel MJR (1992) The dynamics of motion of the South American plate. *Journal of Geophysical Research* 97: 1915–1932.

McGarr A and Gay NC (1978) State of stress in the Earth's crust. *Annual Review of the Earth and Planetary Sciences* 6: 558–562.

McKenzie DP (1982) The relation between fault plane solutions for earthquakes and the directions of the principal stresses. *Bulletin of Seismological Society of America* 59: 591–601.

Michael AJ (1987) The use of focal mechanisms to determine stress: A control study. *Journal of Geophysical Research* 92: 357–368.

Mooney WD, Prodehl C, and Pavlenkova N (2002) Seismic velocity structure of the continental lithosphere from controlled source data. In: Lee WHK (ed.) *International Handbook of Earthquake and Engineering Seismology*, vol. 81A, pp. 887–910. San Diego, CA: Academic Press.

Moos D and Zoback MD (1990) 'Utilization of observations of well bore failure to constrain the orientation and magnitude of crustal stresses: Application to Continental Deep Sea Drilling Project and Ocean Drilling Program Boreholes.' *Journal of Geophysical Research* 95: 9305–9325.

Mount VS and Suppe J (1987) State of stress near the San Andreas Fault: Implications for wrench tectonics. *Geology* 15: 1143–1146.

Mueller B, Zoback ML, Fuchs K, *et al.* (1992) Regional patterns of tectonic stress in Europe. *Journal of Geophysical Research* 92: 11783–11803.

Nakamura K (1977) Volcanoes as possible indicators of tectonic stress orientation – Principle and proposal. *Journal of volcanology and Geothermal Research* 2: 1–16.

Nur A and Walder J (1990) Time-dependent hydraulics of the Earth's Crust. The role of fluids in crustal processes. Washington DC: *National Research Council* 113–127.

Page BM, Thompson GA, and Coleman RG (1998) Late Cenozoic tectonics of the Central and Southern Coast Ranges of California. *Geological Society of America Bulletin* 110: 846–876.

Peska P and Zoback MD (1995) 'Compressive and tensile failure of inclined wellbores and determination of *in situ* stress and rock strength.' *Journal of Geophysical Research* 100(B7): 12791–12811.

Pine RJ, Jupe A, and Tunbridge LW (1990) An evaluation of *in situ* stress measurements affecting different volumes of rock in the Carnmenellis granite. In: Cunha PD (ed.) *Scale Effects in Rock Masses*, pp. 269–277. Rotterdam: Balkema.

Pollack HN, Hurter SJ, and Johnson JR (1993) Heat flow from the Earth's interior: analysis of the global data set. *Reviews of Geophysics* 31: 267–280.

Pavoni N (1961) Faltung durch Horizontal verschiebung. *Ecolgae Geologicae Helvetiae Basel* 54: 515–534.

Pavoni N (1980) Crustal stress inferred from fault-plane solutions of earthquakes and neotectonic deformation in Switzerland. *Rock Mechanics, Supplement* 9: 63–68.

Raleigh CB (1974) Crustal stress and global tectonics. In: International Society for Rock Mechanics and US National Committee for Rock Mechanics (eds.) *Advances in Rock Mechanics: Proceedings of the 3rd Congress, International Society for Rock Mechanics*, vol. 1A, pp. 593–597. Washington, DC: National Academy of Sciences.

Raleigh CB, Healy JH, and Bredehoeft JD (1972) Faulting and crustal stress at Rangely, Colorado. In: Heard HC (ed.) *Geophysical Monograph Series 16:* Flow and Fracture of Rocks, pp. 275–284. Washington, DC: AGU.

Ranalli G and Murphy DC (1987) Rheological stratification of the lithosphere. *Tectonophysics* 132: 281–295.

Richardson RM (1978) Finite element modeling of stress in the Nazca plate: Driving forces and plate boundary earthquakes. *Tectonophys* 50: 223–248.

Richardson RM (1992) Ridge forces, absolute plate motions, and the intraplate stress field. *Journal of Geophysical Research* 97: 1739–1748.

Richardson RM and Cox BL (1984) Evolution of oceanic lithosphere: A driving force study of the Nazca plate. *Journal of Geophysical Research* 89: 10043–10052.
Richardson RM and Reding LM (1991) North American plate dynamics. *Journal of Geophysical Research* 96: 12201–12223.
Richardson RM, Solomon SC, and Sleep NH (1976) Intraplate stress as an indicator of plate tectonic driving forces. *Journal of Geophysical Research* 81: 1847–1856.
Richardson RM, Solomon SC, and Sleep NH (1979) Tectonic stress in the plates. *Reviews of Geophysics* 17: 981–1019.
Sibson RH (1983) Continental fault structure and the shallow earthquake source. *Journal of the Geological Society of London* 5: 741–767.
Solomon SC, Sleep NH, and Richardson RM (1975) On the forces driving plate tectonics: Inferences from absolute plate velocities and intraplate stress. *Geophysical Journal of the Royal Astronomical Society* 42: 769–801.
Sonder LJ (1990) Effects of density contrasts on the orienation of stresses in the lithosphere: Relation to principal stress directions in the Transverse ranges, California. *Tectonics* 9: 761–771.
Stefanick M and Jurdy DM (1992) Stress observations and driving force models for the South American plate. *Journal of Geophysical Research* 97(B8): 11905–11913.
Stein S, Cloetingh S, Sleep NH, and Wortel R (1989) Passive margin earthquakes, stresses and rheology. In: Gregersen S and Basham P (eds.) *Earthquakes at North-Atlantic Passive Margins: Neotectonics and Postglacial Rebound*, *NATO ASI Series C:* pp. 231–259. Dordrecht: Kluwer Academic Publishers.
Stein RS, King GC, and Lin J (1992) 'Change in failure stress on the Southern San Andreas fault system caused by the 1992 magnitude 7.4 Landers earthquake.' *Science* 258: 1328–1332.
Stein S, Sleep NH, Geller RJ, Wang S-C, and Kroeger GC (1979) Earthquakes along the passive margin of eastern Canada. *Geophysical Research Letters* 6: 537–540.
Steinberger B, Schmeling H, and Marquart G (2001) Large-scale lithospheric stress field and topography induced by global mantle circulation. *Earth and Planetary Science Letters* 186: 75–91.
Townend J (2003) *Mechanical Constraints on the Strength of the Lithosphere and plate-bounding Faults. Geophysics*. PhD Thesis, 135, Stanford, CA, Stanford University.
Townend J and Zoback MD (2000) 'How faulting keeps the crust strong.' *Geology* 28(5): 399–402.
Wentworth CM and Zoback MD (1989) The style of late Cenozoic deformation at the eastern front of the California Coast Ranges. *Tectonics* 8: 237–246.
Wessel P and Mueller RD (in press) Treatise on Geophysics, *vol.6: Plate tectonics.*
Wiens DA and Stein S (1985) Implications of oceanic intraplate seismicity for plate stresses, driving forces, and rheology. *Tectonophys* 116: 143–162.
Wortel MJR, Remkes MJN, Govers R, Cloetingh SAPL, and Meijer PT (1991) Dynamics of the lithosphere and the intraplate stress-field. *Philosophical Transactions of the Royal Society of London Series A* 337: 111–126.
Wu P and Johnston P (2000) Can deglaciation trigger earthquakes in North America? *Geophysical Research Letters* 27: 1323–1326.
Zoback ML (1992) First- and second-order patterns of stress in the lithosphere: The World Stress Map project. *Journal of Geophysical Research* 97: 11703–11728. (The current version of the World Stress Map database can be found at: http://www-wsm.physik.uni-karlsruhe.de/).
Zoback MD (2000) Strength of the San Andreas. *Nature* 405: 31–32.
Zoback MD, Apel R, Brudy M, *et al.* (1993) Upper crustal strength inferred from stress measurements to 6 km depth in the KTB borehole. *Nature* 365: 633–635.
Zoback MD and Harjes HP (1997) 'Injection induced earthquakes and crustal stress at 9 km depth at the KTB deep drilling site, Germany.' *Journal of Geophysical Research* 102: 18477–18491.
Zoback MD and Haimson BC (eds.) (1983) *Hydraulic Fracturing Stress Measurements, US National Committee for Rock Mechanics*, 270. Washington, DC: National Press.
Zoback MD and Healy JH (1984) 'Friction, faulting, and *in situ* stresses.' *Annales Geophysicae* 2: 689–698.
Zoback MD and Healy JH (1992) *In situ* stress measurements to 3.5 km depth in the Cajo' n Pass scientific-research borehole: Implications for the mechanics of crustal faulting. *Journal of Geophysical Research* 97: 5039–5057.
Zoback ML and Mooney WD (2003) Lithospheric buoyancy and continental intraplate stress. *International Geology Review* 45: 95–118.
Zoback MD, Moos D, Mastin L, and Anderson RN (1985) Wellbore breakouts and *in situ* stress. *Journal of Geophysical Research* 90: 5523–5530.
Zoback ML, Nishenko SP, Richardson RM, Hasegawa HS, and Zoback MD (1986) Mid-plate stress, deformation, and seismicity. In: Vogt PR and Tucholke BE (eds.) *The Geology of North America, vol. M: The Western North Atlantic Region*, pp. 297–312. Boulder, CO: Geological Society of America.
Zoback ML and Richardson RM (1996) Stress perturbation associated with the Amazonas and other ancient continental rifts. *Journal of Geophysical Research* 101: 5459–5475.
Zoback ML and Thompson GA (1978) Basin and Range rifting in northern Nevada: Clues from a mid-Miocene rift and its subsequent offsets. *Geology* 6: 111–116.
Zoback MD and Townend J (2001) Implications of hydrostatic pore pressures and high crustal strength for the deformation of intraplate lithosphere. *Tectonophysics* 336: 19–30.
Zoback MD, Townend J, and Grollimund B (2002) Steady-state failure equilibrium and deformation of intraplate lithosphere. *International Geology Review* 44: 383–401.
Zoback ML and Zoback MD (1980) State of stress of the conterminous United States. *Journal of Geophysical Research* 85: 6113–6156.
Zoback ML and Zoback MD (1989) Tectonic stress field of the conterminous United States. *Geological Society of America Memoir* 172: 523–539.
Zoback ML, *et al.* (1989) Global patterns of tectonic stress. *Nature* 341: 291–298.
Zoback MD, Zoback ML, Mount VS, *et al.* (1987) New evidence on the state of stress of the San Andreas fault system. *Science* 238: 1105–1111.
Zoback MD and Zoback ML (1991) Tectonic stress field of North America and relative plate motions. In: Slemmons DB, *et al.* (eds.) The Geology of North America, Neotectonics of North America, pp. 339–366. Boulder, CO: Geological Society of America.

Relevant Websites

http://mahi.ucsd.edu – UCSD Department of Mathematics.
http://www-wsm.physik.uni-karlsruhe.de – World Stress Map Project.